

# Modeling the Sun's open magnetic flux and the heliospheric current sheet

J. Jiang, R. Cameron, D. Schmitt and M. Schüssler

*Max-Planck-Institut für Sonnensystemforschung, 37191 Katlenburg-Lindau, Germany*

jiang@mps.mpg.de

## ABSTRACT

By coupling a solar surface flux transport model with an extrapolation of the heliospheric field, we simulate the evolution of the Sun's open magnetic flux and the heliospheric current sheet (HCS) based on observational data of sunspot groups since 1976. The results are consistent with measurements of the interplanetary magnetic field near Earth and with the tilt angle of the HCS as derived from extrapolation of the observed solar surface field. This opens the possibility for an improved reconstruction of the Sun's open flux and the HCS into the past on the basis of empirical sunspot data.

*Subject headings:* solar-terrestrial relations – Sun: activity – Sun: magnetic fields

## 1. Introduction

The Sun's open magnetic flux is the part of its flux which is not contained in closed loops, but extends into the heliosphere. It is the source of the heliospheric magnetic field (HMF) whose variations are an important source of geomagnetic activity (Pulkkinen 2007) and control the production of cosmogenic isotopes by galactic cosmic rays (Beer 2000). A crucial feature of the HMF is the heliospheric current sheet (HCS), the interface separating the opposite polarities of the HMF. The tilt angle of the HCS (defined as the mean of the maximum northern and southern extensions of the HCS) is a key parameter for the modulation of the flux of galactic cosmic rays in the inner heliosphere (Kóta & Jokipii 1983; Ferreira & Potgieter 2004; Alanko-Huotari et al. 2007; Heber et al. 2009).

At a given distance from the Sun, the HMF has an almost uniform magnitude in latitude and longitude (Balogh et al. 1995). Therefore, its radial component near Earth, which has been measured by spacecraft since the 1960s, faithfully represents the Sun's total open flux (Owens et al. 2008; Lockwood et al. 2009). The tilt angle of the HCS could, in principle, be measured by multiple spacecraft orbiting at different heliolatitudes. However, with the exception of the *Ulysses* probe, all measurements of the HMF have been obtained near the ecliptic plane, so that direct measurements of the tilt angle of the HCS are not available most of the time. Therefore, such data are derived by extrapolation of solar surface field maps, such as those taken at the Wilcox Solar Observatory (WSO) since 1976. This yields the current sheet distribution at the source surface, where the field

is assumed to become radial (e.g., Hoeksema et al. 1982). In the inner heliosphere, we may ignore dynamical effects such as the acceleration of slow plasma and the deceleration of fast plasma that occur when neighboring parcels of plasma interact (Riley et al. 2002), so the field lines are assumed to stay purely radial beyond the source surface. Under these conditions, the morphology of the HCS may be inferred from the position of the current sheet at the source surface.

A limitation of this semi-empirical determination of the HCS tilt angle arises from the decreasing reliability of the surface field measurements at higher latitudes and from magnetographic saturation effects, which cannot be corrected without further assumptions. Flux transport models based upon observed large-scale magnetic flux emergence (e.g., in sunspot groups) provide a complementary possibility to obtain information about the high-latitude surface fields, which control the open flux and the HCS tilt angle during solar minimum periods (e.g. Wang et al. 1989a, 2000; Mackay et al. 2002). Schüssler & Baumann (2006) showed that such an approach reproduces well the HMF over multiple solar cycles, provided that the heliospheric current sheet is explicitly included in the field extrapolation (current sheet source surface method, cf. Zhao & Hoeksema 1995a)

The present paper serves a two-fold purpose. Firstly, it extends the study of Schüssler & Baumann (2006) until the current solar minimum period and includes an explicit account of the HCS and its tilt angle, which can be compared with the corresponding observational quantities. Secondly, such comparison provides the validation for the application of these methods to reconstruct the open flux and HCS tilt angle backward in time.

The paper is organized as follows. In Sect. 2, we give the description of the models used. The results are presented in Sect. 3: photospheric flux distributions in Sect. 3.1, the solar open flux in Sect. 3.2, and the heliospheric current sheet in Sect. 3.3. We give our conclusions in Sect. 4.

## 2. Methods

### 2.1. Surface flux transport model

The surface flux transport (SFT) model describes the evolution of the magnetic flux distribution at the solar surface as a combined result of the emergence of bipolar magnetic regions (BMRs), flux cancellation, and transport by surface flows. The evolution of the radially orientated surface field (Wang & Sheeley 1992; Solanki 1993; Petrie & Patrikeeva 2009) is controlled by latitudinal differential rotation and meridional flow, together with turbulent diffusion due to granulation and supergranulation (e.g., Wang et al. 1989b; Mackay et al. 2002).

The SFT uses the radial component of the induction equation in the form

$$\frac{\partial B_r}{\partial t} = -\omega(\theta)\frac{\partial B_r}{\partial \phi} - \frac{1}{R_\odot \sin \theta} \frac{\partial}{\partial \theta} [v(\theta) B_r \sin \theta]$$

$$\begin{aligned}
& + \frac{\eta_h}{R_\odot^2} \left[ \frac{1}{\sin \theta} \frac{\partial}{\partial \theta} \left( \sin \theta \frac{\partial B_r}{\partial \theta} \right) + \frac{1}{\sin^2 \theta} \frac{\partial^2 B_r}{\partial \phi^2} \right] \\
& - D_r(\eta_r B) + S(\theta, \phi, t),
\end{aligned} \tag{1}$$

where  $S(\theta, \phi, t)$  is the source term describing the emergence of new magnetic flux and  $D_r(\eta_r B)$  is the decay term parameterizing the radial diffusion of the magnetic field (Baumann et al. 2006). Following Jiang et al. (2009), the horizontal diffusivity  $\eta_h$  and radial diffusivity  $\eta_r$  are taken as  $600 \text{ km}^2 \text{ s}^{-1}$  and  $100 \text{ km}^2 \text{ s}^{-1}$ , respectively. For the meridional flow  $v(\theta)$ , we adopt the profile

$$v(\theta) = \begin{cases} -v_0 \sin(2.4 * (90^\circ - \theta)) & 15^\circ \leq \theta \leq 165^\circ \\ 0 & \text{otherwise,} \end{cases} \tag{2}$$

where  $v_0 = 11 \text{ m s}^{-1}$ . This profile is largely consistent with helioseismic results (Gizon & Duvall 2004). For the latitudinal differential rotation  $\omega(\theta)$ , we use the empirical profile determined by Snodgrass (1983).

The basis for magnetic flux input to the SFT model by emerging BMRs is the USAF/NOAA sunspot group record <sup>1</sup>. Since a sunspot group typically appears more than once in the record, we consider a group only at the day of its maximum area. Figure 1 gives the monthly number and the latitude distribution (butterfly diagram) of the emerging sunspot groups for the time interval 1976 – 2009, which provide the flux input for the SFT model.

The observed sunspot areas have been converted to the areas of the corresponding BMRs following the procedure of Baumann et al. (2004). We include the magnetic flux contained in faculae and plages by employing the statistical relationship between sunspot area,  $A_s$ , and facular area,  $A_f$ , determined by Chapman et al. (1997),

$$A_f = 414 + 21A_s - 0.0036A_s^2, \tag{3}$$

(in units of millionths of the solar hemisphere) and take  $A_{\text{BMR}} = A_s + A_f$  as area of the corresponding BMR. Since there is no information about the magnetic polarity in the USAF/NOAA data, we use Hale’s polarity law to infer the polarities of the leading and following parts of the BMRs. We resolve the ambiguity arising from the overlap of cycles around activity minima by assuming that BMRs emerging below  $\pm 15^\circ$  latitude during the overlap period belong to the old cycle while all others belong to the new cycle. The angular separation,  $\Delta\beta$  (in degrees), between the leading and following polarity patches of a BMR is assumed to be proportional to the square root of the BMR area (given in square degrees):  $\Delta\beta = 0.6\sqrt{A_{\text{BMR}}}$ . The angular separation is separated into latitudinal and longitudinal components, depending on the BMR tilt angle,  $\gamma$ , with respect to the E–W direction. We assume the relation  $\gamma = 0.15\lambda$ , which is consistent with observational results

---

<sup>1</sup><http://solarscience.msfc.nasa.gov/greenwch.shtml>

(Howard 1991; Sivaraman et al. 1999, Dasi Espuig et al., in preparation)<sup>2</sup>. Finally, we calibrate the conversion factor between BMR area and magnetic flux by matching the observed and simulated values of the disk-averaged unsigned flux density,  $B_s = \int \int |B_r| d\phi \cos(\lambda) d\lambda / 4\pi$ .

## 2.2. Field extrapolation model

In order to determine the coronal and heliospheric magnetic field from its source in the photospheric field, a field extrapolation method is required. For the field distribution on a global scale, the most widely used approach is the potential field source surface (PFSS) model (Schatten et al. 1969; Altschuler & Newkirk 1969). However, the PFSS model (which includes only volume currents beyond the spherical source surface, where the field is assumed to become purely radial) does neither reproduce the latitude-independent radial field found with *Ulysses* (Balogh et al. 1995) nor does it match the measured interplanetary radial field near Earth (Schüssler & Baumann 2006). The current sheet source surface (CSSS) model (Zhao & Hoeksema 1995a,b; Zhao et al. 2002), which explicitly takes into account the existence of the HCS, does not suffer from these deficiencies and provides a reasonable match to the measured quantities (Schüssler & Baumann 2006).

We briefly describe the main features of the CSSS model as follows. To include the effects of volume and sheet currents, the exterior of the Sun is divided into three parts, which are separated by two spherical surfaces, the *cusp surface* at  $r = R_{cs}$ , and the *source surface* at  $r = R_{ss}$  ( $R_{cs} < R_{ss}$ ). In the region inside the cusp surface, the field is potential. In the region between  $R_{cs}$  and  $R_{ss}$ , all flux loops are reconfigured with volume currents and current sheets, so that the field becomes completely open. In the region beyond  $R_{ss}$ , the field is purely radial. Apart from  $R_{cs}$  and  $R_{ss}$ , the third adjustable parameter of the CSSS model is the height scale,  $a$ , of the horizontal current. Following Zhao et al. (2002), we take  $a = 0.2R_{\odot}$  in our calculations. We choose  $R_{ss} = 10.0R_{\odot}$  according to the estimate of Marsch & Richter (1984). The value of  $R_{cs} = 1.8R_{\odot}$  is determined by the comparison between the magnetic flux at the cusp surface and the measured radial field from OMNI2 data in Sect. 3.2.

Technically, the opening of the flux beyond  $R_{cs}$  and the introduction of the current sheet(s) is carried out by first calculating a global potential-field extrapolation for the entire volume above the solar surface. The unsigned radial component of the field at the cusp surface is then used as the boundary condition for calculating a magnetic field distribution between  $R_{cs}$  and  $R_{ss}$  of the form in Bogdan & Low (1986) and used by Zhao & Hoeksema (1995a). The orientation of the field

---

<sup>2</sup>Schüssler & Baumann (2006) attempted to fix the latitude-dependence of the tilt angle independently by calibrating with the longitude-averaged surface field integrated over latitude, viz.  $\int | \int B_r d\phi | \cos(\lambda) d\lambda / 4\pi$ . However, some exploratory experiments we performed have shown that this quantity is rather sensitive to the observed scatter of the BMR tilt angles about the latitude-dependent mean. Since the effect of this scatter is not significant for the quantities that we study in this paper (open flux and tilt of the heliospheric current sheet), we do not consider BMR tilt angle fluctuations here.

lines is then changed where necessary so that the sign and magnitude of the radial field at  $R_{\text{cs}}$  is continuous. The distribution of the field outside  $R_{\text{cs}}$  can then be determined.

### 3. Results

#### 3.1. Photospheric magnetic field distributions

The initial condition for the photospheric flux distribution is the same as the one assumed by Baumann et al. (2004). It satisfies an approximate balance between the effects of poleward meridional flow and equatorial diffusion (van Ballegooijen et al. 1998). The memory of the system regarding the initial field depends on the value of the radial diffusion parameter,  $\eta_r$  (Baumann et al. 2006). We use  $\eta_r = 100 \text{ km}^2 \text{ s}^{-1}$ , which leads to a memory of about 20 yrs. We start all our simulations from the beginning of the USAF/NOAA sunspot group record in 1874, but consider the results only for the time period 1976–2009. Therefore, there is no remaining influence of the initial fields on the results presented below.

The upper panel of Fig. 2 shows a comparison of observed and simulated time evolution of the averaged unsigned flux density at the solar surface,  $B_s$  (defined in Sec. 2.1), which has been used to calibrate the relation between area and magnetic flux of the BMRs providing the input for the flux transport model. Note that, without any other parameter adjustment, the model reproduces well the ratio between the maximum and minimum values as well as the very low surface flux during the current minimum.

The lower panel of Fig. 2 gives the corresponding time evolution of the high-latitude surface field, averaged over the caps poleward of  $\pm 75^\circ$  latitude. The field amplitude and reversal times before 2002 are consistent with the observational results given by Arge et al. (2002). For the current minimum, the reported values of the polar field do not give a consistent picture, reflecting the difficulties and limitations of polar field measurement. Petrie & Patrikeeva (2009) obtained polar fields of 5 – 6 G by analyzing photospheric and chromospheric vector polarimetric data obtained with SOLIS at NSO, which is consistent with our model. On the other hand, MWO magnetograph (Svalgaard et al. 2005) data and more indirect indices (Schatten 2005) suggest that the present polar field could possibly be a factor 2 smaller than that during the previous activity minimum around 1997 (see further discussion in Sect. 3.4).

#### 3.2. Open flux and near-Earth radial field

We can calculate the total open flux  $\Phi_{\text{open}}$  resulting from our extrapolation model by integrating the unsigned radial magnetic field over the source surface, viz.

$$\Phi_{\text{open}}(t) = R_{\text{ss}}^2 \int \int |B_r(R_{\text{ss}}, \lambda, \phi)| d\Omega. \quad (4)$$

Actually, in the CSSS model the open flux is already fixed at the cusp surface,  $R_{cs}$ , smaller values of which leading to a larger amount of open flux. In order to compare with data provided by near-Earth measurements, we also calculate the longitudinally averaged unsigned radial field near Earth (at  $r_E = 1$  AU and  $\lambda = 0$ , thus ignoring the slight variation due to the angle of about 7 degrees between the equatorial plane of the Sun and the ecliptic plane),

$$B_E(t) = \frac{1}{2\pi} \left( \frac{R_{ss}}{r_E} \right)^2 \int_0^{2\pi} |B_r(R_{ss}, 0, \phi, t)| d\phi. \quad (5)$$

Since extrapolations with the CSSS model reproduce the latitude-independence of the radial field at  $r = r_E$  (Schüssler & Baumann 2006), we have  $B_E \simeq \Phi_{open}/(4\pi r_E^2)$  to a high degree of accuracy, so that  $B_E$  also represents the open flux. Similarly, it has been shown that, possibly after some correction for kinematical effects due to the solar wind, the measured radial field near Earth can be taken as a reliable proxy for the total open flux (Owens et al. 2008; Lockwood et al. 2009).

Figure 3 shows 27-day averages of  $B_E$  from our combined SFT/CSSS model (with  $R_{cs} = 1.8R_\odot$ ,  $R_{ss} = 10R_\odot$ ,  $a = 0.2R_\odot$ , red curve) in comparison with the measured radial field from OMNI2 data (blue curve)<sup>3</sup>. Lockwood et al. (2009) have suggested that the observed data better represent the open flux of the Sun if a correction of kinematical effects due to the longitudinal structure of the solar wind is applied. Data modified in this way are also shown in Fig. 3 (green curve).

The phase relation between the solar activity cycle and the near-Earth field (and thus the open flux) is well represented by our model, with  $B_E$  reaching its peak values  $\sim 2 - 3$  yr after activity maximum (cf. Mackay et al. 2002; Wang et al. 2002; Schüssler & Baumann 2006). Including the diffusion in radial direction in the SFT model and the realistic tilt angles of BMRs with respect to the E–W direction are the main reasons that lead to the correct phase relation. The only periods showing a significant disagreement between our model and the data are the ascending phases of the activity cycles, where the model values are too low. Possibly the model misses open flux from small coronal holes at intermediate latitude during this phase. In principle, this could be corrected by putting the cusp surface nearer to the Sun during this cycle phase or by assuming a non-spherical cusp surface. The amplitude of the variation of  $B_E$  is also affected by the value of radial diffusion in the SFT model. However, such parameter tuning would not provide further physical insight while the overall agreement between model and data is already encouraging and sufficient for the purposes of this paper.

### 3.3. Heliospheric current sheet (HCS)

Figure 4 shows the distributions of the magnetic field on the solar surface, on the cusp surface, and on the source surface during typical solar minimum and solar maximum conditions in our

---

<sup>3</sup><http://omniweb.gsfc.nasa.gov/>

coupled SFT/CSSS model. Around solar minimum (left panels), the field at (and outward of) the source surface assumes a ‘split-monopole’ structure (Banaszkiewicz et al. 1998), the HCS separating the two polarities being located near the equatorial plane (Hu et al. 2008). Near activity maximum (right panels), the HCS shows strong excursions in latitude and additional localized current sheets may occur. Apart from the current sheets, the field is always largely latitude-independent. The tilt angle of the HCS is defined by convention as the arithmetic mean of the maximum northward and southward excursions of the HCS (see <http://wso.stanford.edu/Tilts.html>). At the moments shown in Fig. 4, the HCS tilt angle is  $6.5^\circ$  in the activity minimum period and  $71.3^\circ$  in the maximum period.

A comparison between the tilt angle of the HCS resulting from our SFT model with the values derived by PFSS extrapolations of WSO maps of the surface magnetic field is shown in Fig. 5a. The results from our standard CSSS extrapolation (solid red line) do not significantly deviate from those obtained by a PFSS extrapolation of the same SFT results with  $R_{ss} = 3.25R_\odot$  (dashed red line), suggesting that the calculated tilt angle does not sensitively depend on the extrapolation method (in contrast to the distribution of open flux). The other two curves in Fig. 5a represent PFSS extrapolations based on observed photospheric magnetic fields using two different boundary conditions for the photospheric magnetic field (see <http://wso.stanford.edu/Tilts.html>). Both the ‘classic’ (green curve) and ‘new’ (blue curve) extrapolations provided by the WSO website assume that the field is potential between the photosphere and the source surface. The two models differ in the way the photospheric field observations are used as the inner boundary condition and in the height of the source surface. In the ‘classic’ case the surface observations are taken to correspond to the line-of-sight component of the potential field, and the source surface is assumed to be at  $2.5 R_\odot$ . In the ‘new’ model, the observed field is matched to the radial component of the potential field projected onto the line of sight: the assumption is that the field in the photosphere is purely radial and becomes potential only above the surface. Extrapolation for the ‘new’ case exist on the WSO website for source surface heights of  $2.5 R_\odot$  and  $3.25 R_\odot$ . We show the result for  $3.25 R_\odot$  which is claimed to better match Ulysses data.

The result from our model is consistent with both extrapolations. Figure 5b shows the difference between the HCS tilt angle derived from the SFT model with CSSS extrapolation and the other three cases. The agreement with the WSO ‘new’ method is somewhat worse than that of the ‘classic’ method, especially around the activity minimum periods. For physical reasons, it is expected that the ‘new’ method assuming a purely radial photospheric field should be a better representation of the real solar situation (Wang & Sheeley 1992; Petrie & Patrikeeva 2009). Note, however, that inferring the radial field strength from the measured line-of-sight component requires quite large correction factors at high solar latitudes together with the larger uncertainties of the high-latitude data. This suggests that the tilt angles derived from observed synoptic maps during solar minimum periods should be considered with some caution.

### 3.4. The minimum of cycle 23

The current solar minimum appears to be rather extended, with particularly low activity levels. There are indications that the polar field strength is significantly lower than during the two previous minima (e.g. Svalgaard et al. 2005; Schatten 2005; Schrijver & Liu 2008). A low polar field strength would be consistent with the small measured values of the near-Earth interplanetary magnetic field (and thus also the open flux, see Fig. 3) and the relatively large tilt angle of the HCS inferred by the ‘classic’ PFSS extrapolation (blue curve in Fig. 5a). However, the uncertainties in the inferred values of the polar field are large and the HCS tilt angle determined with the (presumably more relevant) ‘new’ PFSS model using a radial-field photospheric boundary condition does not show unusually large minimum values.

Our SFT model yields a polar field during the present minimum which is not significantly weaker than that of the previous minimum (see Fig. 2). The open flux determined from the model is consistent with the low OMNI2 measurements during the current minimum; however, the model results tend to be too low during minima, so that the present agreement might well be fortuitous. The tilt angle of the HCS derived from the SFT model decreases to low values during the current minimum, which is consistent with the ‘normal’ polar field strength that the model yields. The tilt angles inferred from PFSS extrapolations based on observed photospheric field distributions provide a confusing picture (cf. Fig. 5a): while the ‘classic’ line-of-sight boundary condition leads rather large tilt angles, which would be in accordance with a weak polar field, the ‘new’ radial-field boundary condition predicts values not much different from those during previous cycles. As the ‘new’ method is considered to be physically more realistic (Petrie & Patrikeeva 2009), this would dilute the case for an unusually weak polar field during the present minimum.

In the SFT model, the magnitude reached by the polar field in the second half of a cycle crucially depends on the tilt angle (with respect to the East-West direction) of the emerging bipolar magnetic regions during the cycle. We have assumed the same relationship,  $\gamma = 0.15\lambda$ , between tilt angle and emergence latitude for all cycles considered. However, the analysis of sunspot group data indicates that the factor of proportionality in this relation may actually vary from cycle to cycle (Dasi Espuig et al., in preparation). Systematically smaller tilt angles during cycle 23 could lead to a unusually weak polar field during the present minimum. Alternatively, Schrijver & Liu (2008) proposed an increased strength of the diverging meridional flow near the equator as an explanation for the weak polar field.

## 4. Conclusions

We have simulated the temporal evolution of the Sun’s total open magnetic flux and the heliospheric current sheet (HCS) since 1976 by coupling a surface flux transport (SFT) model and the current sheet source surface (CSSS) extrapolation method, using the observed sunspot groups to provide the magnetic flux input for the model. We draw the following conclusion from our



results:

1) The simulated open flux matches the OMNI2 data quite well, except for systematically lower values in the ascending phase of the activity cycle. This is consistent with the view that the solar open flux is largely determined by the instantaneous photospheric sources.

2) At the source surface, the magnetic field satisfies the ‘split monopole’ configuration suggested by the *Ulysses* out-of-ecliptic measurements.

3) The temporal variation of the tilt angle of the HCS from the SFT/CSSS model matches the values derived from potential field source surface(PFSS) extrapolations of the observed photospheric magnetic field. The best agreement is found for the ‘classic’ line-of-sight condition.

4) The conditions during the present minimum period of cycle 23 as provided by the SFT/CSSS model are similar to those at previous minima: the polar field has about the same strength as that of cycle 22, the tilt angle of the HCS is small, and the open flux is roughly at the level of the last minimum. Since 2007, however, the HCS tilt angle has deviated significantly from the WSO PFSS values with line-of-sight boundary condition (‘classic’ case) and approached those with the ‘new’ radial boundary condition. These results may well be affected by a systematic variations of the sunspot group tilts with respect to the E–W direction from cycle to cycle, as indicated by recent analysis of sunspot observations.

5) In spite of some deviations in detail, the overall agreement of the model results with observationally inferred values of open flux and current sheet geometry is encouraging. It opens the possibility to extend the model backward in time by using the sunspot group record since 1874. This will be the topic of a subsequent paper.

Acknowledgments: Y.-M. Wang kindly provided the observational datasets of the averaged unsigned photospheric field shown in Fig. 2. M. Lockwood kindly provided the kinematically corrected OMNI2 data shown in Fig. 3.

## REFERENCES

- Alanko-Huotari, K., Usoskin, I. G., Mursula, K., & Kovaltsov, G. A. 2007, *Adv. Space Res.*, 40, 1064
- Altschuler, M. D., & Newkirk, G. 1969, *Sol. Phys.*, 9, 131
- Arge, C. N., Hildner, E., Pizzo, V. J., & Harvey, J. W. 2002, *J. Geophys. Res.*, 107, 1319
- Balogh, A., Smith, E. J., Tsurutani, B. T., Southwood, D. J., Forsyth, R. J., & Horbury, T. S. 1995, *Science*, 268, 1007
- Banaszkiewicz, M., Axford, W. I., & McKenzie, J. F. 1998, *A&A*, 337, 940

- Baumann, I., Schmitt, D., Schüssler, M., & Solanki, S. K. 2004, *A&A*, 426, 1075
- Baumann, I., Schmitt, D., & Schüssler, M. 2006, *A&A*, 446, 307
- Beer, J. 2000, *Space Sci. Rev.*, 94, 53
- Bogdan, T. J., & Low, B. C. 1986, *ApJ*, 306, 271
- Chapman, G. A., Cookson, A. M., & Dobias, J. J. 1997, *ApJ*, 482, 541
- Ferreira, S. E. S., & Potgieter, M. S. 2004, *ApJ*, 603, 744
- Gizon, L. & Duvall, T. L. 2004, in *Multi-Wavelength Investigations of Solar Activity*, ed. Stepanov, A. V., Benevolenskaya, E. E., & Kosovichev, A. G., *IAU Symp.*, 223, 41
- Heber, B., Kopp, A., Gieseler, J., Müller-Mellin, R., Fichtner, H., Scherer, K., Potgieter, M. S., & Ferreira, S. E. S. 2009, *ApJ*, 699, 1956
- Hoeksema, J. T., Wilcox, J. M., & Scherrer, P. H. 1982, *J. Geophys. Res.*, 87, 10331
- Howard, R. F. 1991, *Sol. Phys.*, 136, 251
- Hu, Y. Q., Feng, X. S., Wu, S. T., & Song, W. B. 2008, *J. Geophys. Res.*, 113, A03106
- Jiang, J., Cameron, R., Schmitt, D., & Schüssler, M. 2009, *ApJ*, 693, L96
- Kóta, J., & Jokipii, J. R. 1983, *ApJ*, 265, 573
- Leighton, R. B. 1964, *ApJ*, 140, 1547
- Lockwood, M., Rouillard, A. P., Finch, I., & Stamper, R. 2006, *J. Geophys. Res.*, 111, A09109
- Lockwood, M., Rouillard, A. P., & Finch, I. D. 2009, *ApJ*, 700, 937
- Mackay, D. H., Priest, E. R., & Lockwood, M. 2002, *Sol. Phys.*, 209, 287
- Marsch, E., & Richter, A. K. 1984, *J. Geophys. Res.*, 89, 5386
- Owens, M. J., Arge, C. N., Crooker, N. U., Schwadron, N. A., & Horbury, T. S. 2008, *J. Geophys. Res.*, 113, 12103
- Petrie, G. J. D., & Patrikeeva, I. 2009, *ApJ*, 699, 871
- Pulkkinen, T. 2007, *Living Rev. Solar Phys.*, 1, 4
- Riley, P., Linker, J. A., & Mikić, Z. 2002, *J. Geophys. Res.*, 107, 1136
- Schatten, K., 2005, *Geophys. Res. Lett.*, 32, 21106
- Schatten, K. H., Wilcox, J. M., & Ness, N. F. 1969, *Sol. Phys.*, 6, 442

- Schüssler, M., & Baumann, I. 2006, *A&A*, 459, 945
- Schrijver, C. J., & Liu, Y. 2008, *Sol. Phys.*, 252, 19
- Sivaraman, K. R., Gupta, S. S., & Howard, R. F. 1999, *Sol. Phys.*, 189, 69
- Snodgrass, H. B. 1983, *ApJ*, 501, 866
- Solanki, S. K., 1993, *Space Sci. Rev.*, 63, 1
- Svalgaard, L., Cliver, E. W. & Kamide, Y. 2005, *Geophys. Res. Lett.*, 32, L01104
- van Ballegooijen, A. A., Cartledge, N. P., & Priest, E. R., 1998, *ApJ*, 501, 866
- Wang, Y.-M., Nash, A. G., & Sheeley, N. R., Jr. 1989a, *Sol. Phys.*, 347, 529
- Wang, Y.-M., Nash, A. G., & Sheeley, N. R., Jr. 1989b, *Science*, 245, 712
- Wang, Y.-M., & Sheeley, N. R., Jr. 1992, *ApJ*, 392, 310
- Wang, Y.-M., Sheeley, N. R., Jr., & Lean, J. 2000, *Geophys. Res. Lett.*, 27, 621
- Wang, Y.-M., Sheeley, N. R., Jr., & Lean, J. 2002, *ApJ*, 580, 1188
- Zhao, X. P., Hoeksema, J. T. 1995a, *J. Geophys. Res.*, 100, 19
- Zhao, X. P., Hoeksema, J. T. 1995b, *Space Sci. Rev.*, 72, 189
- Zhao, X. P., Hoeksema, J. T., & Rich, N. R. 2002, *Adv. Space Res.*, 29, 411

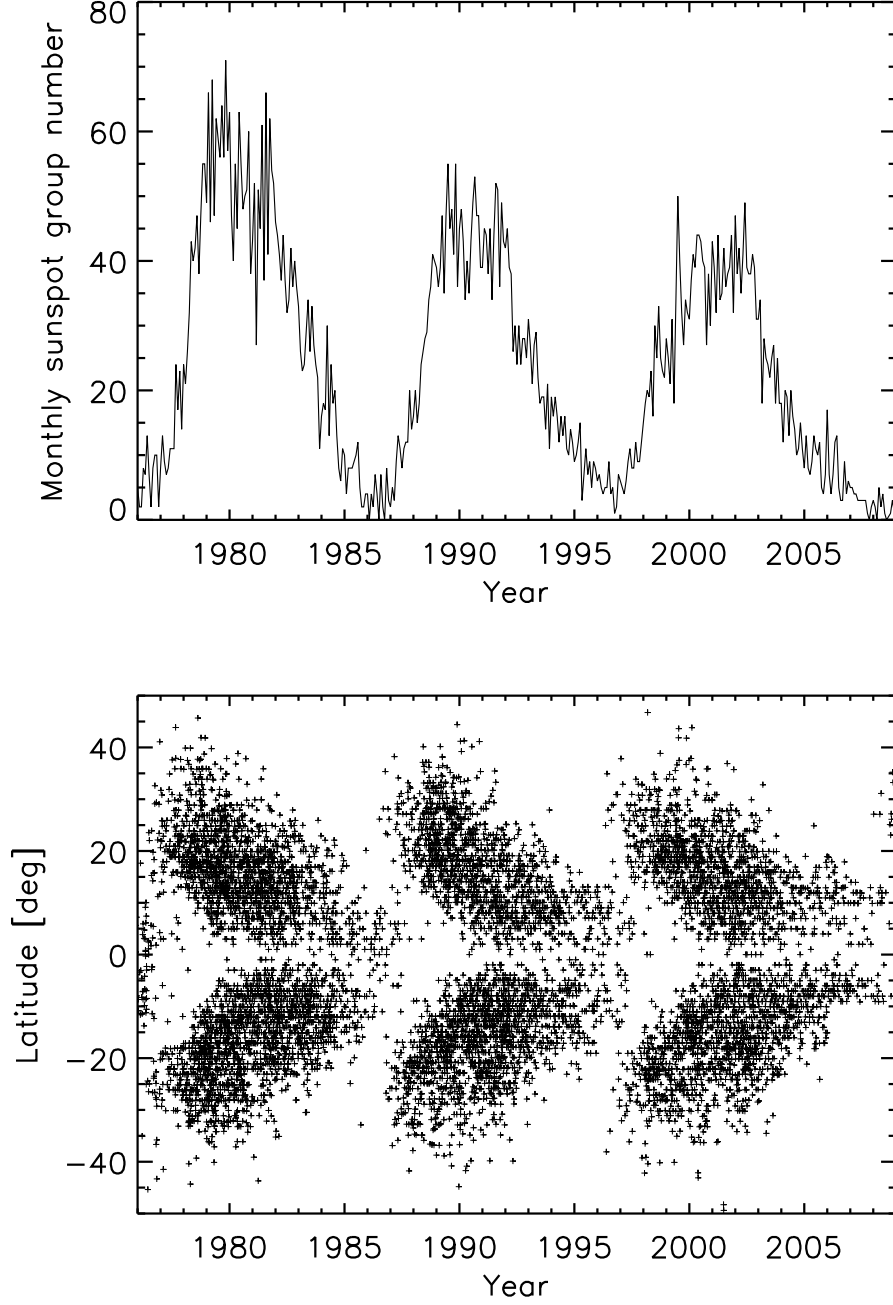


Fig. 1.— Number of sunspot groups per month (upper panel) and time-latitude plot of the emerging sunspot groups (lower panel) that constitute the input sequence of BMRs to the SFT model . Data source: USAF/NOAA.

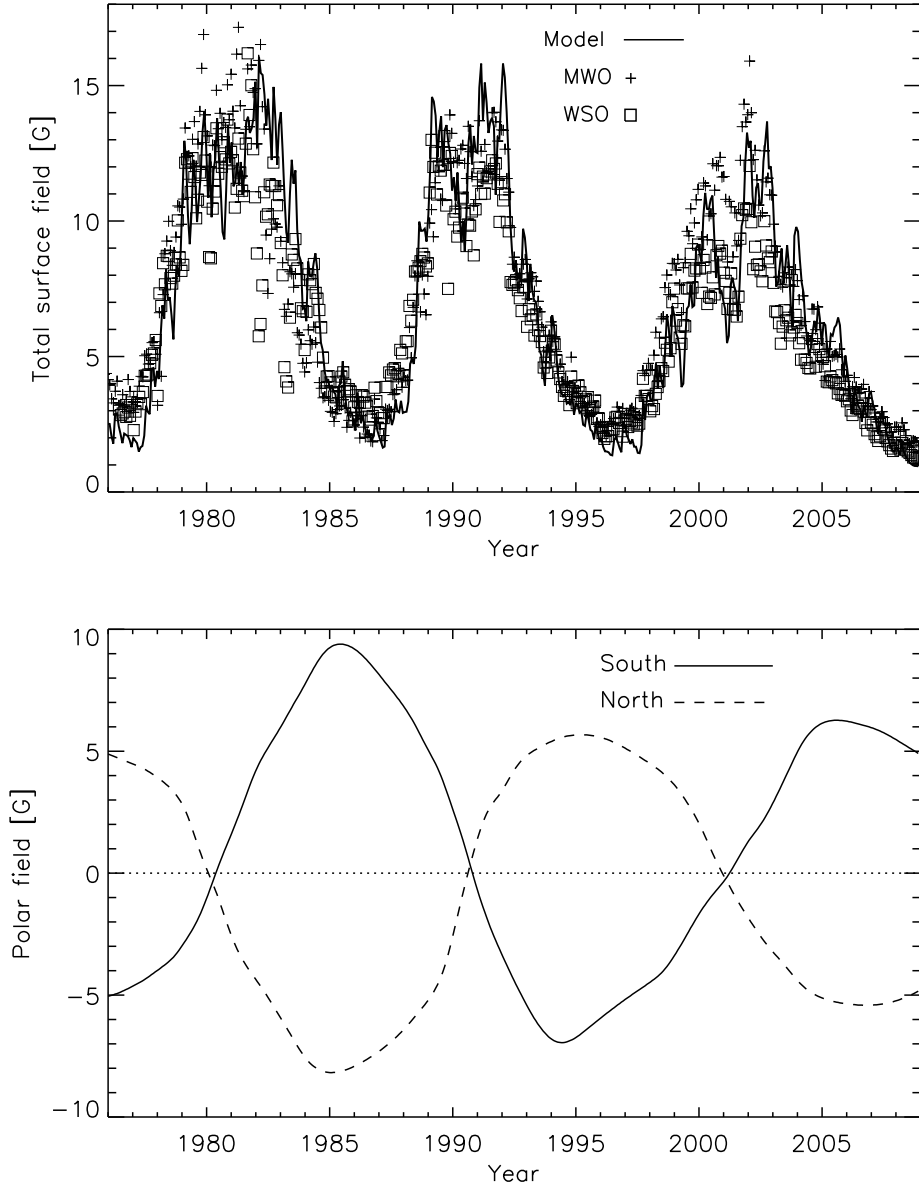


Fig. 2.— Upper panel: Averaged unsigned photospheric field as a function of time. The symbols show the observed data from the Wilcox and Mount Wilson observatories (averaged over Carrington rotations). The solid curve represents 27-day averages from the SFT simulation. Lower panel: The temporal evolution of south (solid curve) and north (dashed curve) polar fields (averages poleward of  $\pm 75^\circ$  latitude).

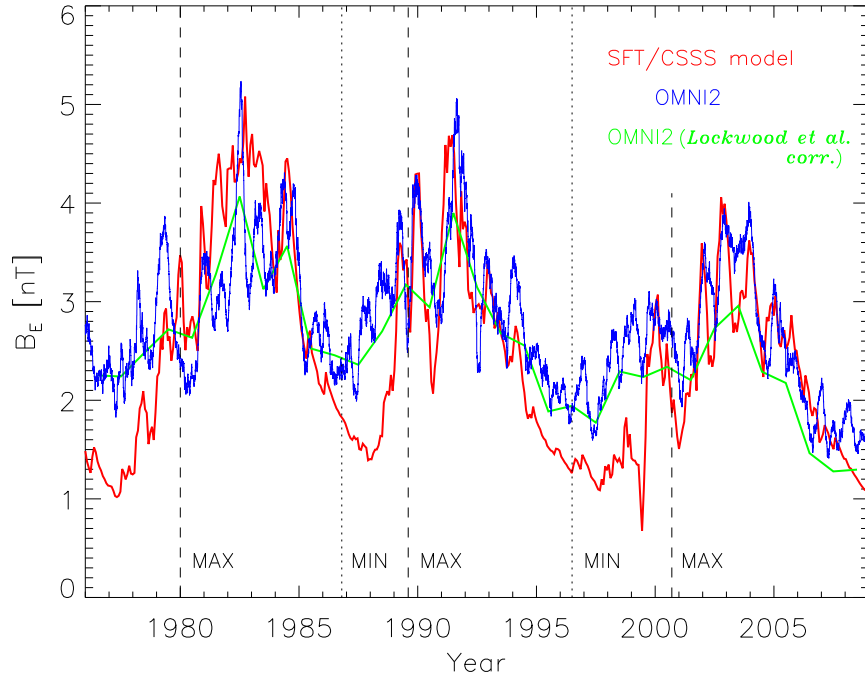


Fig. 3.— Temporal evolution of the unsigned radial field at 1 AU. Shown are the results derived from the SFT/CSSS model (red curve) in comparison with near-Earth measurements (blue curve). The latter have been obtained by first averaging the (signed) OMNI2 data over 1-day intervals to remove small-scale fluctuations (Lockwood et al. 2006) and then carrying out a 3-month running average of the unsigned values. The green curve represents yearly averages of the measurements after applying a kinematic correction (Lockwood et al. 2009) to remove effects due to the longitudinal structure in the solar wind. Dashed and dotted vertical lines indicate the epochs of solar cycle maxima and minima, respectively.

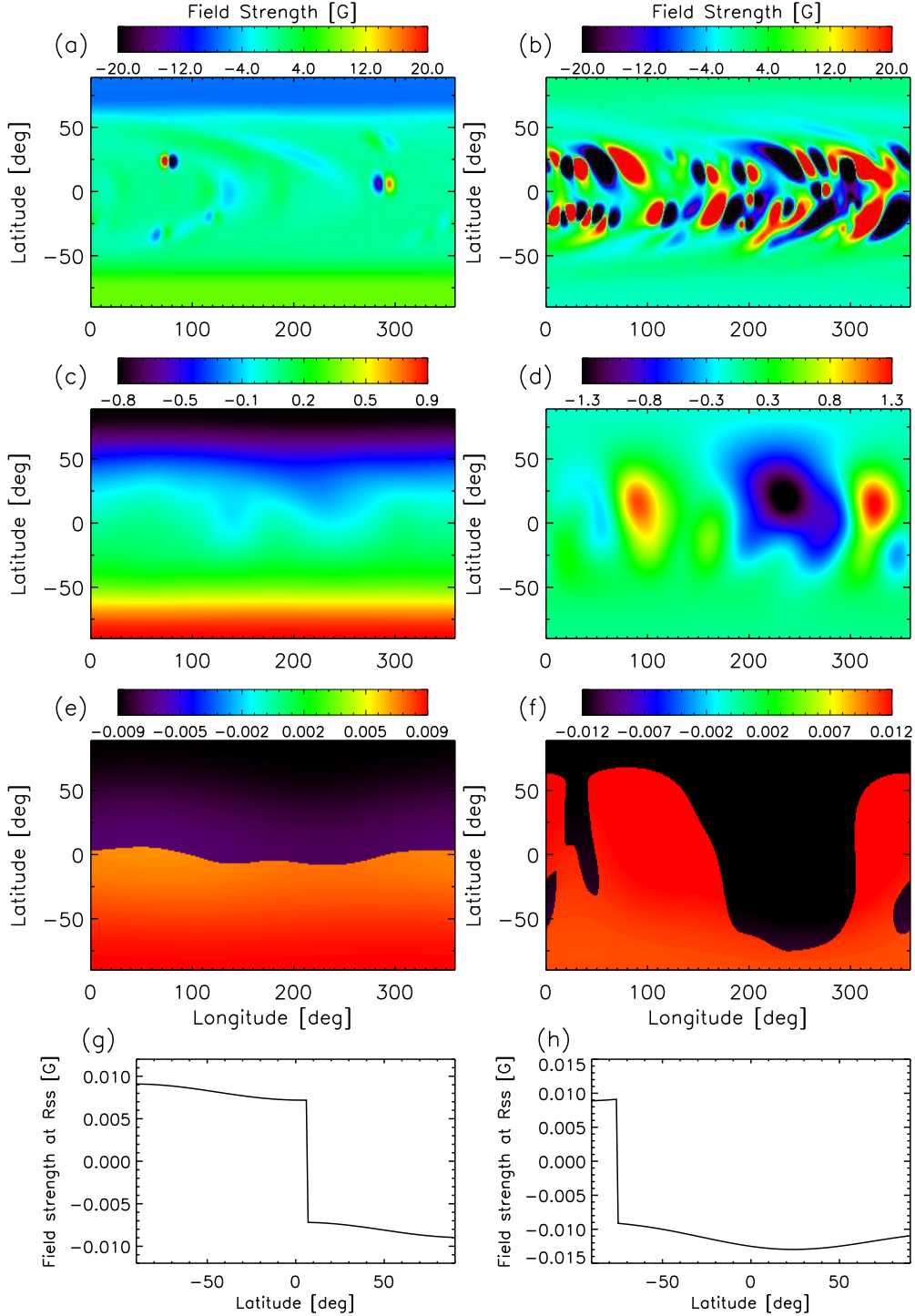


Fig. 4.— Magnetic field distributions at solar minimum (left panels, in 1987.2) and solar maximum (right panels, in 2000.5) resulting from the coupled SFT/CSSS model. Maps of the radial field are shown at the solar surface (a,b), at the cusp surface at  $R_{cs} = 1.8R_{\odot}$  (c,d), and at the source surface at  $R_{ss} = 10R_{\odot}$  (e,f). Panels g and h show latitude profiles of the field strength at the source surface, taken at the longitude with the largest latitude excursion of the heliospheric current sheet (HCS).

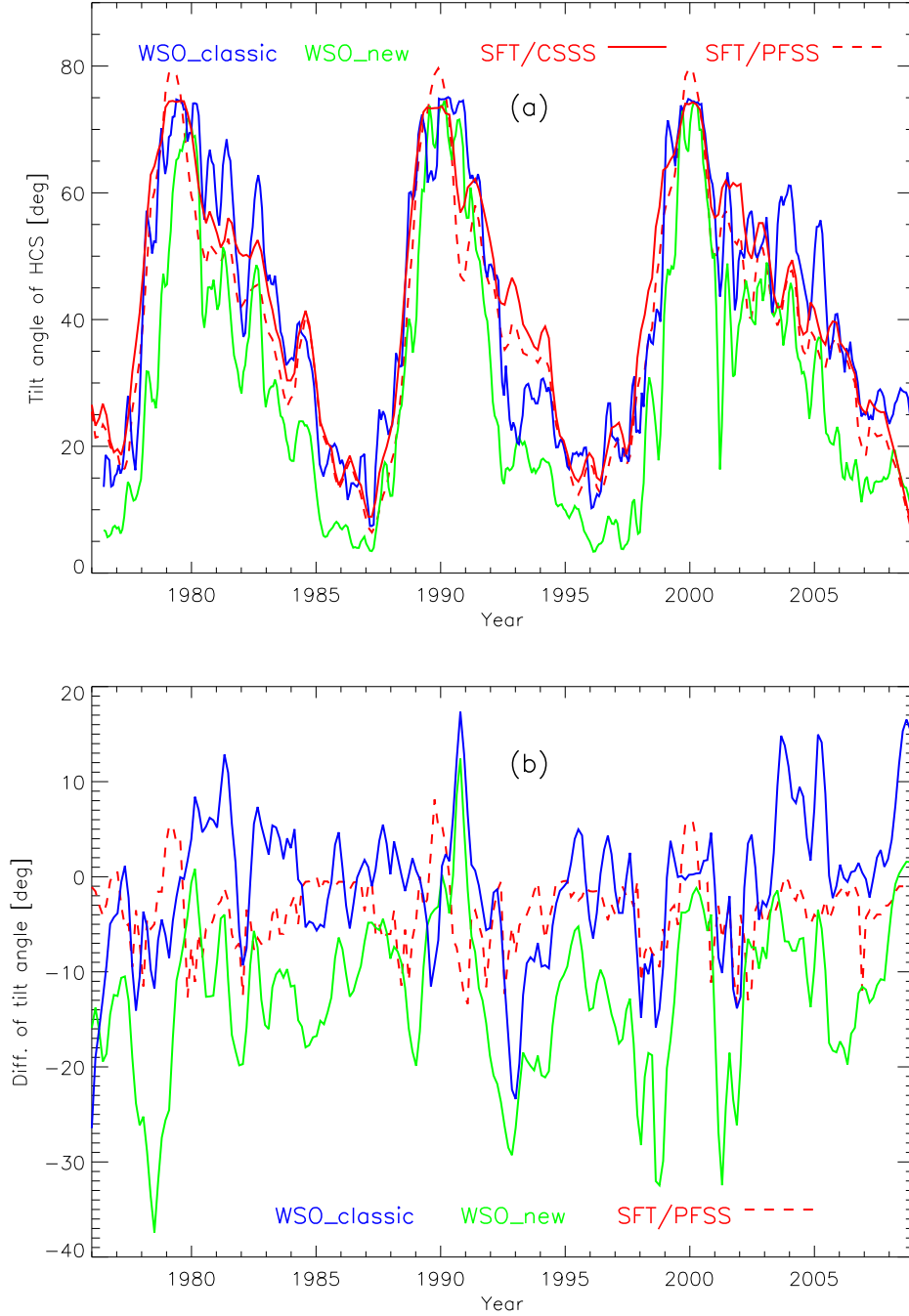


Fig. 5.— (a) Temporal evolution of the HCS tilt angle. Solid red curve: SFT result with CSSS extrapolation ( $a = 0.2R_{\odot}$ ,  $R_{cs}=1.8R_{\odot}$ ,  $R_{ss}=10R_{\odot}$ ); dashed red curve: SFT result with PFSS extrapolation ( $R_{ss} = 3.25R_{\odot}$ ); blue curve: PFSS extrapolation of WSO synoptic maps with line-of-sight field boundary condition (‘classic’ model,  $R_{ss} = 2.5R_{\odot}$ ); green curve: PFSS extrapolation of WSO synoptic maps with radial field boundary condition (‘new’ model,  $R_{ss} = 3.25R_{\odot}$ ). The data for the blue and green curves have been obtained from the WSO website (<http://wso.stanford.edu/Tilts.html>). (b) The difference between the HCS tilt angle from the SFT/CSSS and the three other methods shown in the same color scheme as used in (a).